A Theoretical Study of Benzhydroxamic Acid Binding Modes in Horseradish Peroxidase

Yan-Tyng Chang,*,† Nigel C. Veitch,‡ and Gilda H. Loew†

Contribution from the Molecular Research Institute, 845 Page Mill Road, Palo Alto, California 94304-1011, and Jodrell Laboratory, Royal Botanic Gardens, Kew, Richmond, Surrey TW9 3DS, England

Received November 13, 1997. Revised Manuscript Received February 10, 1998

Abstract: In this study, the substrate binding sites and mode of binding of benzhydroxamic acid (BHA) in the low-spin cyanide-ligated form of horseradish peroxidase isoenzyme C (HRP-C) have been identified and characterized using the X-ray crystallographic structure of HRP-C in the substrate-free form, in combination with the programs AUTODOCK and AMBER. Two criteria were used to select the most favorable binding site: the interaction energy of BHA with the protein and the mobility of BHA in each binding site. Using these criteria, the binding site located on the distal side of the heme and surrounded by His42, Arg38, Pro139, Leu138, Ala140, Phe68, Pro141, Gly69, Phe179, Phe41, Asn70, and Ser73 was found most promising. Computed distances between atoms in BHA and atoms in residues of HRP-C/CN were, in general, in good agreement with a subset of corresponding distances derived from ^{1}H NMR data. In addition, two strong H bonds of BHA, with Arg38 and the N atom of the cyanide ligand, and two polar interactions of BHA, with His42 and Pro139, were found, consistent with the relatively high binding affinity of BHA for HRP-C/CN. The second most favorable binding site identified was located toward the proximal side of the heme at a distance of only 10 Å from the first binding site, as described above, suggesting it as a temporary storage place for the radical produced by oxidation of the first substrate molecule. This small displacement would allow accommodation of a second substrate molecule in the first site and dimerization to occur after the second substrate radical is formed through a second one-electron oxidation step. Although it is not known whether BHA forms dimers due to oxidation by HRP-C, other phenolic substrates that do form dimers may occupy both the primary binding site, where oxidation occurs, and the radical holding site, to facilitate dimer formation.

Introduction

Horseradish peroxidase is a member of the superfamily of heme peroxidases which includes enzymes of plant, fungal, and bacterial origin.[1] The number of peroxidase genes identified in horseradish (*Armoracia rusticana*) and the number of peroxidases sequenced either classically or from cDNA indicate that there are at least 10 different isoenzymes, the majority of which appear to be localized in the root. Among them, the highly abundant C isoenzyme (HRP-C) has been a major focus of studies concerned with structure−function relationships within the peroxidase family of enzymes.[2−5] It is now believed that, in the catalytic cycle of a typical heme peroxidase, a concerted two-electron oxidation of the ferric resting form of the enzyme by hydrogen peroxide produces the catalytically active enzyme species known as compound I. Typical peroxidase substrates are phenols, aromatic amines, and aromatic sulfonates. The catalytically active compound I species performs a one-electron oxidation of such substrates, yielding a free radical product and another enzyme intermediate, known as compound II. Compound II then performs a second sequential one-electron oxidation of another substrate molecule, leading again to an initial radical product, with the enzyme returning to its ferric resting state. There are several possible fates for the free radical products formed initially, depending on their chemistry. These radicals may (i) dimerize, (ii) react with another substrate molecule, (iii) attack another species causing co-oxidation, (iv) reduce molecular oxygen to superoxide, or (v) be scavenged by molecular oxygen to form a peroxyl radical.[5]

Despite the existence of the X-ray crystallographic structures of several peroxidases, including cytochrome *c* peroxidase,[6] ascorbate peroxidase,[7] lignin peroxidase,[8] manganese peroxidase,[9] fungal peroxidases from *Arthromyces ramosus*[10] and from *Coprinus cinereus*,[11] peanut peroxidase,[12] and, most recently, horseradish peroxidase isoenzyme C (Brookhaven Protein Data Bank accession code 1ATJ),[13] only two of these have ever been

* To whom correspondence should be addressed. Tel.: (650) 424-9924. Fax: (650) 424-9501. E-mail: chang@purisima.molres.org.

† Molecular Research Institute.

‡ Royal Botanic Gardens.

(1) Welinder, K. G. *Curr. Opin. Struct. Biol.* **1992**, *2*, 388−393.

(2) Dunford, H. B.; Stillman, J. S. *Coord. Chem. Rev.* **1976**, *19*, 187−251.

(3) Dunford, H. B. *Adv. Inorg. Biochem.* **1982**, *4*, 41−68.

(4) Hewson, W. D.; Hager, L. P. In *The Porphyrins*; Dolphin, D., Ed.; Academic Press: New York, 1979; Vol. 7, pp 295−332.

(5) Dunford, H. B. In *Peroxidases in Chemistry and Biology*; Everse, J., Everse, K. E., Grisham, M. B., Eds.; CRC Press: Boca Raton, FL, 1991; Vol. II, pp 1−24.

(6) Poulos, T. L.; Freer, S. T.; Alden, R. A.; Edwards, S. L.; Skogland, U.; Takio, K.; Eriksson, B.; Xuong, N.; Yonetani, T.; Kraut, J. *J. Biol. Chem.* **1980**, *255*, 575−580.

(7) Patterson, W. R.; Poulos, T. L. *Biochemistry* **1995**, *34*, 4331−4341.

(8) Poulos, T. L.; Edwards, S. L.; Wariishi, H.; Gold, M. H. *J. Biol. Chem.* **1993**, *268*, 4429−4440.

(9) Sundaramoorthy, M.; Kishi, K.; Gold, M. H.; Poulos, T. L. *J. Biol. Chem.* **1994**, *269*, 32759−32767.

(10) Kunishima, N.; Fukuyama, K.; Matsubara. H.; Hatanaka, H.; Shibano, Y.; Amachi, T. *J. Mol. Biol.* **1994**, *235*, 331−344.

(11) Petersen, J. F. W.; Kadziola, A.; Larsen, S. *FEBS Lett.* **1994**, *339*, 291−296.

(12) Schuller, D. J.; Ban, N.; van Huystee, R. B.; McPherson, A.; Poulos, T. L. *Structure* **1996**, *4*, 311−321.

S0002-7863(97)03907-3 CCC: $15.00
Published on Web 05/13/1998

resolved in a complex with a substrate molecule. The first example is the cytochrome *c* peroxidase/cytochrome *c* complex[14] and the second the *A. ramosus* peroxidase/BHA complex, solved only recently.[15] Thus, the number, location, and nature of the substrate binding sites remain among the major unresolved aspects within the three classes of the plant peroxidase superfamily of enzymes and, in particular, of the classical plant peroxidases themselves.

In the past, knowledge about the binding site(s) has been obtained indirectly as evidence from NMR studies,[16−34] from substrate and product specificity studies,[35−37] and from studies of covalent phenyl radical adducts.[38−41] The consensus of opinion in the case of HRP-C is that typical aromatic donor molecules such as phenols bind to a site at the exposed heme edge near to the δ-meso proton C20H and heme methyl C18H_3 groups (see Figure 1 for heme nomenclature) of the porphyrin ring, while their protons are located at distances between 8 and 12 Å from the heme iron atom.[17] This evidence suggests that the mode of oxidation is the transfer of an electron from the substrate to the porphyrin ring. Other high-affinity/low-efficacy substrates such as BHA also appear to bind near to heme methyl C18H_3 and in the distal heme pocket.[21,28] In addition, the facts that, in a typical peroxidase reaction, two substrate molecules are oxidized sequentially and that these two radical products form dimers imply a possible radical holding site to which the first oxidation product moves to allow the second substrate to be oxidized by compound II.

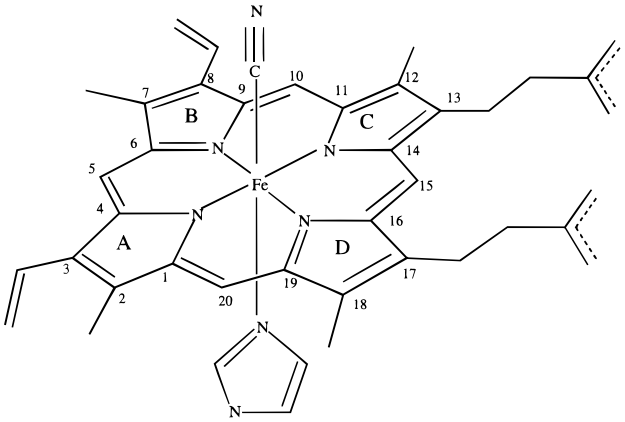

Figure 1. Heme nomenclature.

Despite the fact that some knowledge regarding the binding site(s) in HRP-C is available, a detailed description regarding the residues that form the binding site(s), the binding mode(s) of substrates, and the interaction between residues and substrates is still lacking. In this paper, to obtain such a detailed description, a theoretical study of the possible binding modes of BHA in HRP-C/CN is presented, using the recently resolved substrate-free X-ray structure of HRP-C.[13] This BHA/HRP-C/CN ternary complex was chosen because (1) BHA has relatively small K_d values (i.e., high binding affinity) compared to other typical aromatic donors that have K_d values in the millimolar range, (2) the ternary complex has been extensively used for NMR studies, as chemical shift changes induced on BHA binding are not comprised by the additional factor of apparent spin- and coordination-state changes which occur with the resting state enzyme, and (3) experimental data examining BHA binding to cyanide-ligated mutant HRP-C enzymes with Phe substitutions at sequence positions 41, 68, 142, 143, and 179 are available.[20,22,23,25] The existence of NMR experimental data for this BHA/HRP-C/CN complex thus allows independent assessment of the binding site selected by purely theoretical methods. The successful validation of the results obtained by the study of BHA reported here indicate that the methods used can be applied to identify and characterize the binding modes of other substrates in HRP-C. Given the increasing number of industrial, biomedical, and biotechnological applications of HRP that exploit a wide variety of substrates, such theoretical prediction of the binding modes of the substrates will be invaluable. In addition, the same methodology can also be applied to the many other peroxidases with structures known only in substrate-free forms.

Methods

Substrate Parametrization. The coordinates of the BHA molecule used were those of an energy-optimized structure obtained previously[42] from an ab initio RHF/6-31G* calculation. The atomic charges of BHA

(13) Gajhede, M.; Schuller, D. J.; Henriksen, A.; Smith, A. T.; Poulos, T. L. *Nat. Struct. Biol.* **1997**, *4*, 1032−1038.
(14) Pelletier, H.; Kraut, J. *Science* **1992**, *258*, 1748−1755.
(15) Itakura, H.; Oda, Y.; Fukuyama, K. *FEBS Lett.* **1997**, *412*, 107−110.
(16) Morishima, I.; Ogawa, S. *J. Biol. Chem.* **1979**, *254*, 2814−2820.
(17) Sakurada, J.; Takahashi, S.; Hosoya, T. *J. Biol. Chem.* **1986**, *261*, 9657−9662.
(18) Veitch, N. C.; Williams, R. J. P. *Eur. J. Biochem.* **1990**, *189*, 351−362.
(19) Veitch, N. C.; Williams, R. J. P. In *Biochemical, molecular and physiological aspects of plant peroxidases*; Lobarzewski, J., Greppin, H., Penel, C., Gaspar, T., Eds.; University of Geneva: Geneva, Switzerland, 1991; pp 99−109.
(20) Veitch, N. C.; Williams, R. J. P.; Bray, R. C.; Burke, J. F.; Sanders, S. A.; Thorneley, R. N. F.; Smith, A. T. *Eur. J. Biochem.* **1992**, *207*, 521−531.
(21) Veitch, N. C.; Williams, R. J. P. *Eur. J. Biochem.* **1995**, *229*, 629−640.
(22) Veitch, N. C.; Williams, R. J. P.; Bone, N. M.; Burke, J. F.; Smith, A. T. *Eur. J. Biochem.* **1995**, *233*, 650−658.
(23) Veitch, N. C.; Gilfoyle, D. J.; White, C. G.; Smith, A. T. In *Plant Peroxidases: Biochemistry and Physiology*; Obinger, C., Burner, U., Ebermann, R., Penel, C., Greppin, H., Eds.; University of Geneva: Geneva, Switzerland, 1996; pp 1−6.
(24) Veitch, N. C. *Biochem. Soc. Trans.* **1995**, *23*, 232−240.
(25) Veitch, N. C.; Gao, Y.; Smith, A. T.; White, C. G. *Biochemistry* **1997**, *36*, 14751−14761.
(26) Thanabal, V.; De Ropp, J. S.; La Mar, G. N. *J. Am. Chem. Soc.* **1987**, *109*, 7516−7525.
(27) De Ropp, J. S.; Yu, L. P.; La Mar, G. N. *J. Biomol. NMR* **1991**, *1*, 175−190.
(28) La Mar, G. N.; Hernandez, G.; De Ropp, J. S. *Biochemistry* **1992**, *31*, 9158−9168.
(29) Chen, Z.; De Ropp, J. S.; Hernandez, G.; La Mar, G. N. *J. Am. Chem. Soc.* **1994**, *116*, 8772−8783.
(30) La Mar, G. N.; Chen, Z.; Vyas, C. K.; McPherson, A. D. *J. Am. Chem. Soc.* **1995**, *117*, 411−419.
(31) De Ropp, J. S.; Chen, Z.; La Mar, G. N. *Biochemistry* **1995**, *34*, 13477−13484.
(32) De Ropp, J. S.; Mandal, P.; Brauer, S. L.; La Mar, G. N. *J. Am. Chem. Soc.* **1997**, *119*, 4732−4739.
(33) Burns, P. S.; Williams, R. J. P.; Wright, P. E. *J. Chem. Soc., Chem. Commun.* **1975**, 795−796.
(34) Banci, L.; Bertini, I.; Bini, T.; Tien, M.; Turano, P. *Biochemistry* **1993**, *32*, 5825−5831.
(35) Casella, L.; Poli, S.; Gullotti, M.; Selvaggini, C.; Beringhelli, T.; Marchesini, A. *Biochemistry* **1994**, *33*, 6377−6386.
(36) Dexter, A. F.; Lakner, F. J.; Campbell, R. A.; Hager, L. P. *J. Am. Chem. Soc.* **1995**, *117*, 6412−6413.
(37) Lee, K.; Brand, J. M.; Gibson, D. T. *Biochem. Biophys. Res. Commun.* **1995**, *212*, 9−15.
(38) Ortiz de Montellano, P. R. *Acc. Chem. Res.* **1987**, *20*, 289−294.
(39) Samokyszyn, V. M.; Ortiz de Montellano, P. R. *Biochemistry* **1991**, *30*, 11646−11653.
(40) Ortiz de Montellano, P. R. *Annu. Rev. Pharmacol. Toxicol.* **1992**, *32*, 89−107.
(41) Gilfoyle, D. J.; Rodriguez-Lopez, J. N.; Smith, A. T. *Eur. J. Biochem.* **1996**, *236*, 714−722.
(42) Zhao, D.; Gilfoyle, D. J.; Smith, A. T.; Loew, G. H. *Proteins Struct. Funct. Genet.* **1996**, *26*, 204−216.

were obtained by fitting the resulting electrostatic potential using the CHELPG method.

Modification of the Known HRP-C Structure to the Ferric HRP-C/CN Form. The coordinates of HRP-C in its resting state were obtained from the X-ray structure resolved by Gajhede et al.[13] The enzyme contains a resting-state protoporphyrin IX heme unit, residues 1−306, two Ca^{2+}, and 128 structural waters. Since the NMR studies were performed for the BHA/HRP-C/CN,[17,19,20,22,23,25,26,28,30] a cyanide-ligated form of HRP-C was constructed by adding CN^- to the heme iron.

Characterization of Complexes of BHA with Ferric HRP-C/CN. The goal of this work was to find all plausible binding sites for BHA in HRP-C/CN and develop criteria for selecting the most favorable among them. Thus, in the first step of this process, 10 different initial positions of BHA were chosen. Among them, (1) four were chosen with varying distances from 5 to 12.9 Å between the center of mass of BHA and the heme C18 methyl carbon atom and (2) six sites near the surface of HRP-C were chosen visually, each originally occupied by 2−5 water molecules. The program AUTODOCK[43] was then used to find the best docking mode of BHA in each of these 10 initial substrate−enzyme complexes. Molecular dynamics simulations were performed subsequently to characterize further the most favorable complexes identified using AUTODOCK, thus allowing selection among them of the most plausible binding site and binding mode. Both procedures are described in detail below.

Optimization of the 10 Local Binding Modes Using AUTODOCK. Probing the 10 plausible docking modes of BHA in HRP-C/CN was performed systematically using the program AUTODOCK. This program uses the united atom force field of AMBER 4.1.[44] Thus, to use this program, HRP-C/CN had to be represented by this force field. The force field parameters of a united-atom heme with a His and a CN^- as its fifth and sixth ligands, respectively, were developed by (1) taking parameters previously developed in this laboratory for a resting-state united-atom His-ligated heme[45] and (2) modifying these parameters due to the addition of CN^- ligand. All of the crystal waters were then removed. A 3D box of dimensions $x = 66.0$ Å, $y = 76.8$ Å, and $z = 66.0$ Å was used to enclose the entire HRP-C system and to allow ∼5 Å distance from any atom in HRP-C to the edge of the box. A grid spacing of 0.6 Å was used to create grid points within the box. Since the BHA ligand contains only four different atom types, namely, H, C, N, and O, four grid maps representing the interaction potential of each atom type in a grid point with the enzyme were generated using the autogrid program of AUTODOCK.

AUTODOCK was then used independently 10 times, commencing with each of the 10 initial positions of BHA in order to find the best docking mode in each of the 10 local regions. The program uses a simulated annealing algorithm to search for the best translational and rotational binding mode of the substrate in the host enzyme. During the search process, the substrate BHA is treated as a rigid molecule. For each of the 10 initial complexes, this search was repeated 50 times. Each search was started with a low initial temperature of 500 RT, to adequately sample the binding modes in a local region. The reduction factor was set to 0.95, and, for each search, 500 cycles were used. The final positions of the ligand at the end of each of the 50 searches were collected. The interaction energy and docking mode of BHA with HRP-C/CN from each of the 50 searches were calculated and compared, and the complex with the best interaction energy among the 50 for each of the 10 initial complexes was retained. These interaction energies and positions of the substrate in the best mode obtained from each of the 10 initial positions were then compared, and the five unique modes with the most favorable interactions were selected for further analysis using molecular dynamics simulations.

MD Simulations of the Five Most Favorable BHA/HRP-C/CN Complexes. For each BHA/HRP-C/CN complex selected for detailed analysis, molecular dynamics simulations were performed using the program package AMBER 4.1.[44] For the BHA substrate, all residues, and the cyanide-ligated heme, all atoms including hydrogens were included explicitly. The force field parameters for an all-atom CN^-- and His-bound heme were taken from a previous study performed in this laboratory[42] that used AMBER 4.0 and modified slightly for this study in order to use AMBER 4.1. For each docking mode selected, the coordinates of BHA obtained from AUTODOCK were used. Crystal water molecules, if any, that resided in the position where BHA was to be placed were removed. Since none of the plausible substrate binding sites was completely buried in the interior of the enzyme, a proper solvent medium was needed. Therefore, the substrate and CN^--bound all-atom HRP-C system was solvated with layers of water molecules with a thickness of ∼7 Å surrounding the whole complex. This procedure typically resulted in a total of ∼11 500 atoms, of which ∼4800 atoms are from the BHA/HRP-C/CN ternary complex, ∼400 atoms are from the crystal waters, and the remaining ∼6300 atoms are from the solvent water molecules. This system was then used in the energy minimization and MD simulations without the application of additional boundaries. Unconstrained energy minimization of the whole system was then performed for 3000 steps. During the subsequent MD simulations, a long nonbonding cutoff of 13 Å was used. A dielectric constant of 1 was used since explicit solvents were included in the simulations. The whole system was coupled to a heat bath with its temperature kept at 300 K during the entire course of the simulation. To gradually bring the system to equilibrium, in the beginning of the MD simulations, all atoms in the system were constrained with a harmonic constraint of 10 kcal/Å^2 for 1 ps. This constraint was gradually reduced to 5.0, 1.0, 0.5, and 0.1 kcal/Å^2 for a total of additional 5 ps for all of the atoms in the system. Then, a 180-ps MD simulation was performed, with a harmonic constraint of 0.1 kcal/Å^2 applied only to the oxygen atoms of solvent water molecules in order to prevent solvent water from evaporating. During the 180-ps simulations, the coordinates of all atoms were recorded at 0.1-ps intervals for further analysis.

Table 1. Interaction Energy (in kcal/mol) of the Lowest Energy Docking Mode of BHA in HRP-C/CN from Each Simulated Annealing Run Using AUTODOCK[a]

complex	initial BHA COM	BHA COM in lowest energy mode	interaction energy
1	(−8.0, 73.0, 28.0)	(−13.0, 71.2, 29.3)[b]	−42.0
2	(−13.3, 67.7, 30.8)	(−13.1, 71.2, 29.3)[b]	−41.6
3	(−8.0, 78.0, 23.0)	(−13.5, 71.3, 29.1)[b]	−39.7
4	(−11.8, 79.8, 34.2)	(−11.7, 79.7, 34.0)	−38.2
5	(−6.8, 58.1, 43.0)	(−11.8, 42.9, 39.3)	−38.0
6	(−5.9, 63.8, 30.8)	(−11.9, 72.3, 28.7)[c]	−37.1
7	(−27.7, 51.0, 33.5)	(−27.7, 55.2, 30.3)[d]	−37.0
8	(−17.5, 50.8, 34.7)	(−27.5, 55.5, 30.3)[d]	−36.7
9	(−14.0, 38.0, 25.5)	(−17.7, 41.0, 21.7)	−34.9
10	(−4.1, 55.7, 22.3)	(−3.0, 63.1, 19.2)	−34.7

[a] The position of heme iron in the X-ray structure is at (−12.8, 66.4, 35.4), and that of the heme methyl C18 carbon atom is at (−11.0, 71.2, 33.5). [b] Binding modes generated from initial complexes **1**−**3** are identical. [c] Binding mode generated has same position but different orientation compared to complexes **1**−**3**. [d] Binding modes generated from initial complexes **7** and **8** are identical.

Results and Discussion

A. Identification of Plausible Binding Modes of BHA in HRP-C/CN. In the search for plausible binding modes of BHA, 10 initial binding positions were selected, as discussed in the Methods section, and 10 runs using AUTODOCK were performed, each with one of the 10 different initial BHA positions. These different initial positions are represented by the initial BHA center of mass (COM) position in column 2 of Table 1. The best binding mode obtained from each of the 10 initial positions is given by the BHA center of mass position in column 3 of Table 1. The interaction energy obtained with AUTODOCK between BHA and HRP-C/CN in the best binding mode from each initial position is also listed in the last column of Table 1, in decreasing order of the interaction energies.

(43) Morris, G. M.; Goodsell, D. S.; Huey, R.; Olson, A. J. *AUTODOCK*, version 2.2; The Scripps Research Institute: La Jolla, CA, 1994.

(44) Pearlman, D. A.; Case, D. A.; Caldwell, J. W.; Ross, W. S.; Cheatham, T. E.; Ferguson, D. M.; Seibel, G. L.; Singh, U. C.; Weiner, P.; Kollman, P. A. *AMBER 4.1*, UCSF: San Francisco, CA, 1995.

(45) Du, P. Private communication.

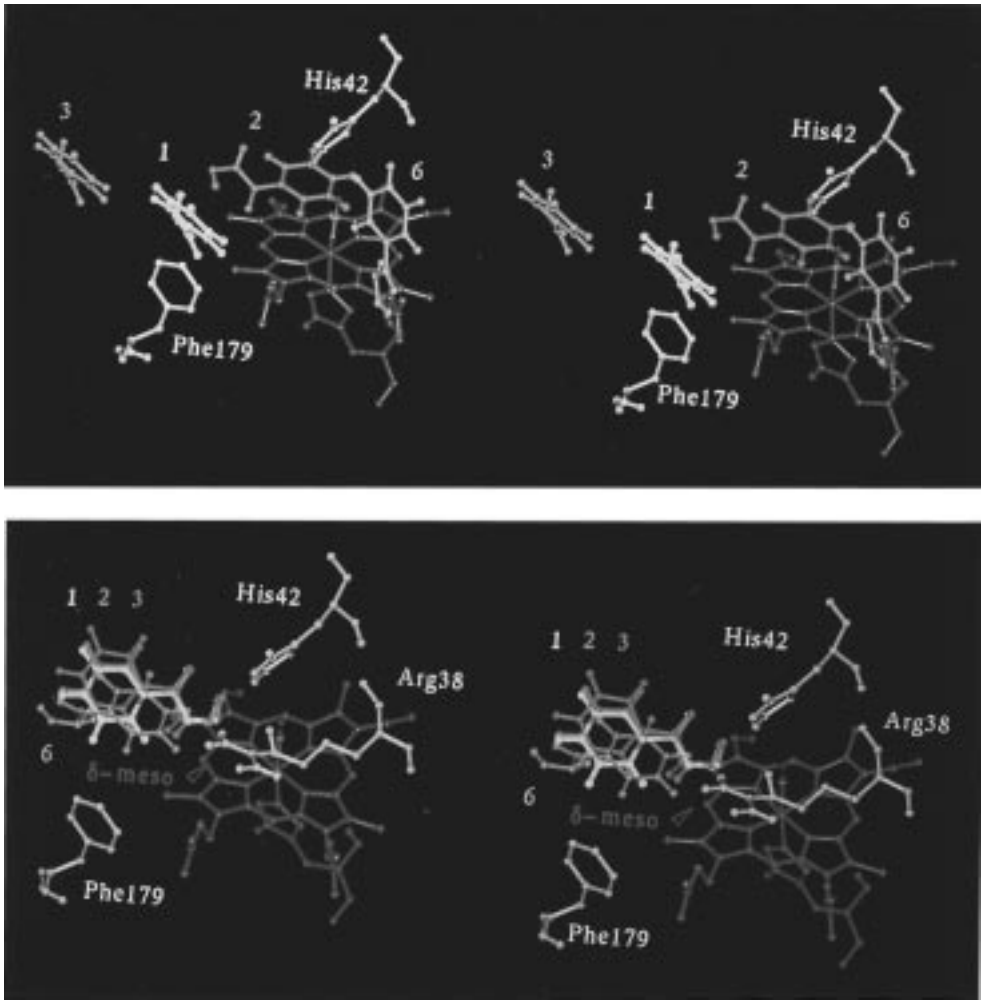

Figure 2. (a, top) Stereoview of the initial position of BHA in complexes **1**−**3** and **6**. (b, bottom) Stereoview of the final positions of these complexes. **1**, Yellow; **2**, cyan; **3**, green; **6**, magenta.

Figure 2 shows the initial and final positions of BHA from the four initial binding modes near the heme, namely complexes **1**, **2**, **3**, and **6**. The initial positions of BHA in complexes **1**, **2**, and **3** place the center of mass of BHA within 6.5, 5.0, and 12.9 Å, respectively, from the position of the heme methyl C18 carbon atom. However, as shown in Table 1 and Figure 2b, the resulting best binding modes from these three complexes converge to a common optimized complex, with (1) similar interaction energy, (2) a common binding site, (3) similar center of mass positions of BHA, 4.7 Å (for complexes **1** and **2**) and 5.1 Å (for complex **3**) away from the heme methyl C18 carbon atom and on the distal side of the heme plane, and (4) the same binding orientation of BHA. In this orientation, the aromatic ring of BHA points away from the heme iron and is surrounded by Phe68, Ala140, Pro141, and Phe179, while the polar end of BHA points in toward the heme iron. After optimization with AUTODOCK, the other initial position, represented by complex **6**, in which BHA is 9.4 Å away from the heme methyl C18 methyl atom, ends with BHA in the same binding site as those from initial complexes **1**−**3**. In contrast, however, BHA is oriented differently in this site, such that its aromatic ring points in toward the heme iron. The interaction energy of this binding mode is less favorable compared to that obtained from the most favorable mode starting from complexes **1**−**3**, as shown in Table 1.

The six additional initial surface positions 4, 5, 7, 8, 9, and 10 of BHA that were chosen visually, each originally occupied by 2−5 water molecules, are shown in Figure 3a, together with the initial docking mode 1 for comparison. Figure 3b shows the best binding mode resulting from each of these six initial positions. As can be seen in Table 1, the best surface-accessible binding mode generated is that from initial complex **4**. The binding energy is only 4 kcal/mol less than that calculated for the most favorable mode. In this site (4), BHA is only ∼10 Å away from BHA in the most favorable site (1), shown in these figures for comparison. The position of BHA in each of the remaining five optimized complexes is much farther away from BHA in complexes **1**−**3**. Specifically, the distances are 30.0, 21.4, 21.8, 31.5, and 16.4 Å for complexes **5**, **7**, **8**, **9**, and **10**, respectively.

The robust nature of the AUTODOCK procedures can be judged by the facts that (i) complexes **1**, **2**, **3**, and **6**, which have very different initial BHA positions, end with the same binding position near the heme, with three of them having identical binding orientations, (ii) two initially different complexes involving surface accessible sites, **7** and **8**, also result in identical optimized binding sites, and (iii) in three out of the six initial complexes near the surface, **4**, **7**, and **9**, BHA remains within 6 Å of its initial position, while in the remaining three complexes, **5**, **8**, and **10**, the procedures locate the best binding modes, with BHA more than 8 Å away from its initial position.

Comparison of the properties of the 10 binding modes generated from AUTODOCK allows the selection of the most promising one. It is the common binding site and common BHA orientation identified from the three initially different positions of complexes **1**−**3**. Not only is the interaction energy

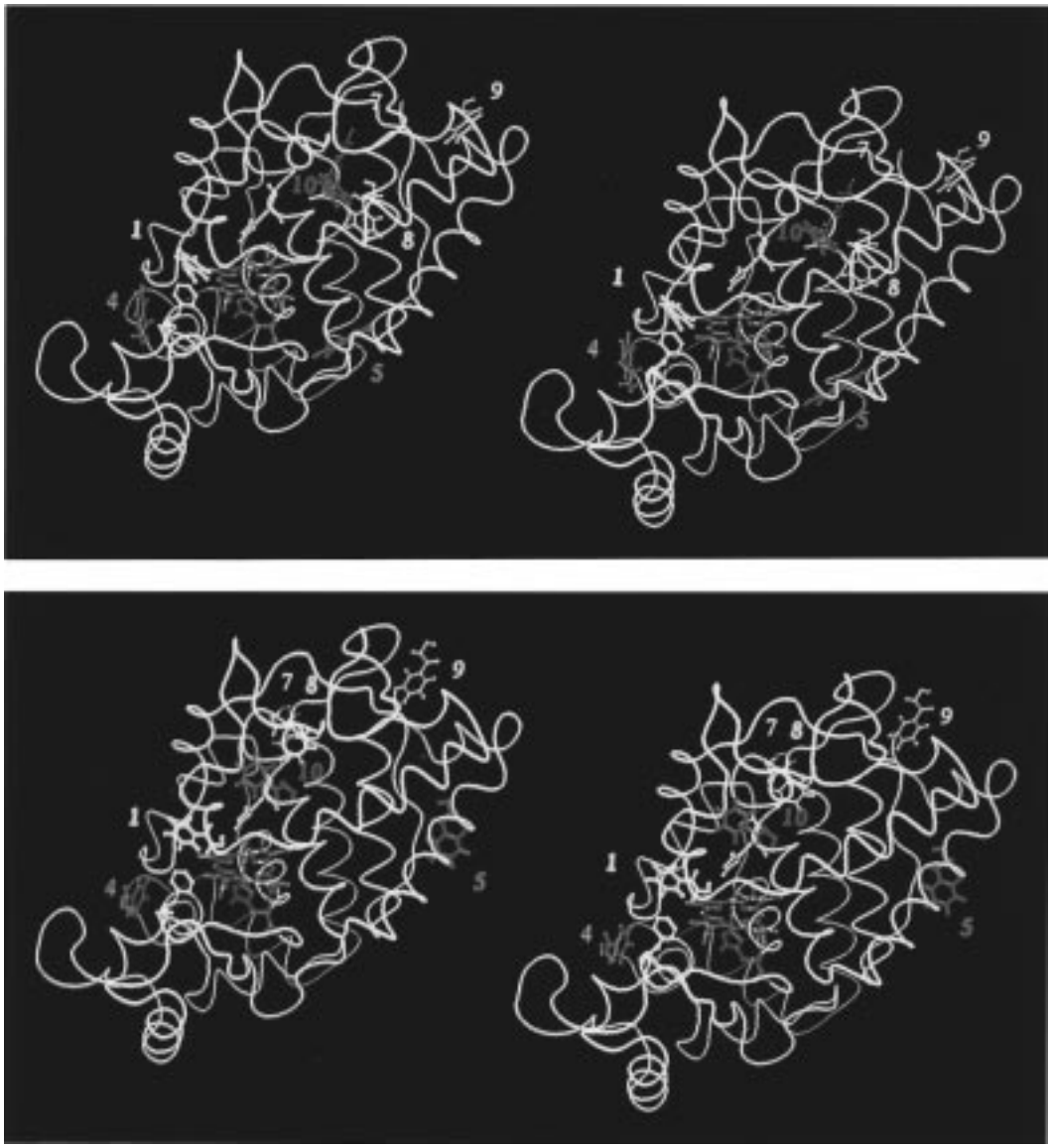

Figure 3. (a, top) Stereoview of the initial positions of BHA in complexes **1**, **4**, **5**, **7**−**10**. (b, bottom) Stereoview of the best docking modes for these complexes. **1**, Yellow; **4**, green; **5**, cyan; **7**, purple; **8**, brown; **9**, magenta; and **10**, blue.

of BHA with HRP-C/CN in this binding mode the most favorable, but also the binding position of BHA in this mode agrees with the observation that BHA binds to HRP-C at a location near to heme methyl $C18H_3$.[17]

To further assess the validity of the most favorable binding mode found using the AUTODOCK procedure, molecular dynamics simulations of the five BHA/HRP-C/CN complexes with the most favorable interaction energies were performed. Specifically, these five complexes were the common unique complex generated from initial complexes **1**−**3** and the best complexes generated from initial complexes **4**−**7**. These optimized complexes were each subjected to 180-ps MD simulations using procedures described in the Methods section. Figure 4 shows the total energy, the kinetic energy, and the potential energy of the whole system with BHA docked in HRP-C/CN using the best docking mode obtained from initial complex **1**. It shows that the system has equilibrated after ∼80 ps of simulations. Examination of the energetics for the other four complexes during their MD simulations showed similar equilibration behavior. Analysis of these five runs was, therefore, performed using the coordinates obtained from the last 100 ps of simulations. First, the MD average interaction energy of BHA with its environment was calculated and decomposed into different contributions, as summarized in Table 2. In this table, the MD average interaction energies of BHA with individual residues that are within 7 Å from the center of mass of BHA are listed in descending order. Also listed are the interaction energies of BHA with all of the remaining residues (others) in HRP-C, with all crystal water molecules, and with all solvent molecules. The total interaction energy of BHA with its environment is also listed. As shown in Table 2, the interaction energy between BHA and all amino acids in HRP-C/CN exhibits the following trend: complex **1** (−48.9 kcal/mol) > complex **4** (−31.2 kcal/mol) > complex **6** (−25.2 kcal/mol) > complex **5** (−23.5 kcal/mol) > complex **7** (−21.6 kcal/mol). This result is similar to the descending order obtained from AUTODOCK. However, the energy difference between these five binding modes is much more significant from the MD simulations than from AUTODOCK. The interaction energy between BHA and the solvent water molecules represents the other significant contribution to the overall interaction of BHA with its environment. This interaction is much more important for complexes **4**−**7** since (i) in complexes **4**, **5**, and **7**, BHA is docked near the surface of HRP-C and (ii) in complex **6**, the polar end of BHA is pointing out toward the crystal waters and the solvent waters.

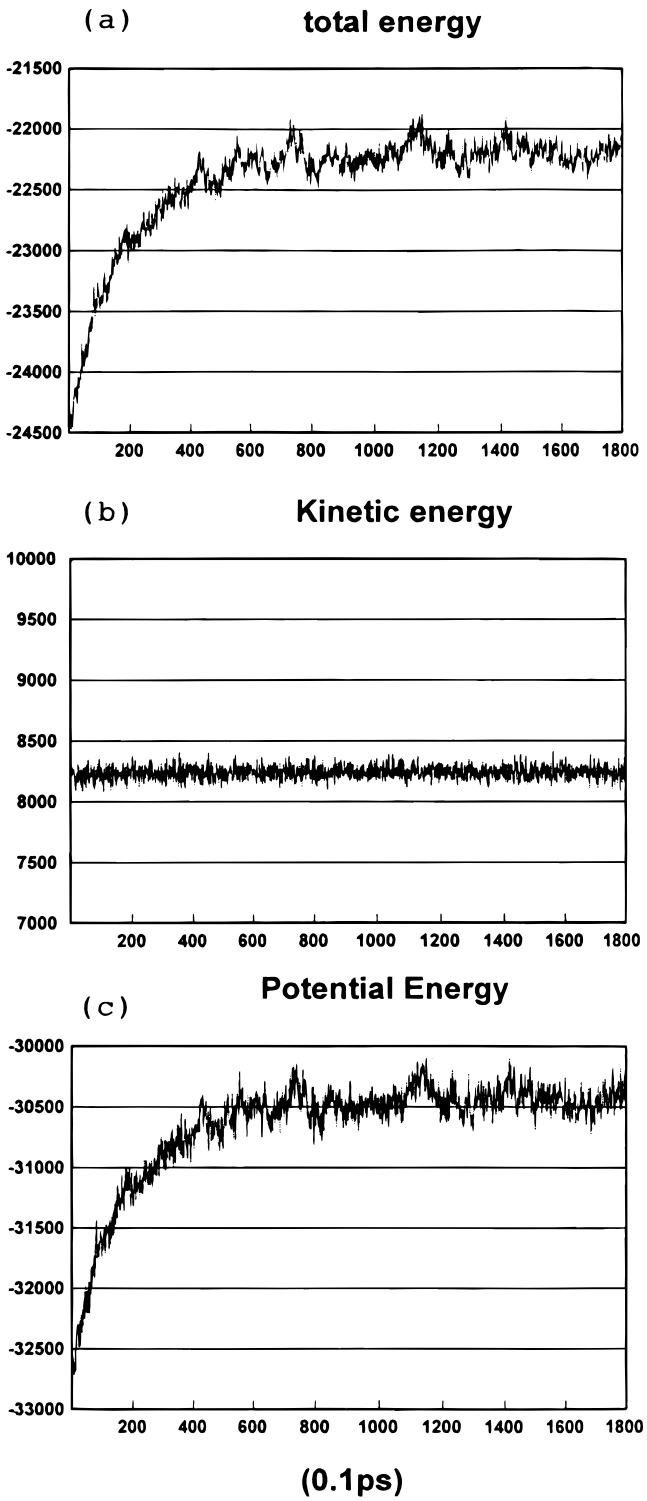

Figure 4. (a) Total energy, (b) kinetic energy, and (c) potential energy of the BHA-bound HRP-C/CN system, using the binding mode generated from complex **1**.

In addition to the comparison of the interaction energy, the stability of BHA in these five plausible binding modes was evaluated by calculating the *B* factor of each BHA atom (*B* factor $= 8\pi^2\langle\Delta r^2\rangle/3$, where Δr is the atomic deviation at a certain time from the MD average position) during the last 100 ps of each run. The *B* factor for the whole BHA molecule obtained from the average of these atomic *B* factors is listed in Table 2. These results show that BHA in the binding mode generated from complex **1** is the most stable, followed by complexes **4**, **6**, **7**, and **5**.

Assessment of both the interaction energy between BHA and HRP-C/CN and the stability of BHA in each site indicates that the unique common binding mode obtained from initial complexes **1**−**3** for BHA is still the most promising. Figure 5 shows BHA in this binding mode with its surrounding residues (within 7 Å), which include His42, Arg38, Pro139, Leu138, Ala140, Phe68, Pro141, Gly69, Phe179, Phe41, Phe142, Asn70, and Ser73.

The second most promising binding mode is represented by complex **4**. Although the interaction energy between BHA and HRP-C/CN in this binding mode is ∼18 kcal/mol less than that of complex **1**, its total interaction including solvent is only ∼4 kcal/mol less. It also has the second best interaction energy with the protein alone: about 6 kcal/mol better than complex **6** and about 10 kcal/mol better than complexes **5** and **7**. The BHA binding pocket of complex **4** is shown in Figure 6. In this site, BHA (labeled as BHA-4) is surrounded by Asp182, Phe142, Phe179, Pro141, Arg178, Gln245, Ile180, Met181, Phe187, and Ile244 and is located on the proximal side of the heme plane, as opposed to BHA in complex **1**, which is located on the distal side of the heme. The distance between the COM of BHA in complex **1** (labeled as BHA-1), shown in this figure for comparison, and BHA in complex **4** (labeled as BHA-4) is only ∼10 Å. On the basis of these results, it is proposed that distal binding site 1 is the site of oxidation of aromatic donor substrates. For most aromatic donor substrates (not including BHA) that are known to form dimers due to oxidation by HRP-C, binding site 4 may serve as a temporary storage site for the radical product from the first substrate molecule, allowing oxidation of the second substrate in the complex **1** binding mode. Dimerization of substrate radicals could then occur easily after the second substrate is oxidized.

The third most promising binding mode is represented by complex **6**. This is located at the same site as that from complex **1**, but with an opposite binding orientation. As shown in Table 2, the mobility of BHA, as represented by the *B* factor, in this mode is comparable to that in complex **4**. However, the interaction energy between BHA and HRP-C/CN in this binding mode is much less than that from complexes **1** and **4**. Inspection of Table 2 indicates that the residues which interact significantly with BHA in complex **1** and complex **6** are the same. The 24 kcal/mol reduction in interaction energy between BHA and HRP-C/CN in complex **6** compared to complex **1** is due principally to the unfavorable interactions between BHA and the His42 and Arg38 side chains in complex **6**, as opposed to the strong attractive interactions in complex **1**.

The two other surface binding sites for BHA do not appear to be important. Based on results from MD simulations, the interaction energy between BHA and HRP-C/CN in complex **5** and in complex **7** is more than 25 kcal/mol less than that in complex **1**. Furthermore, even with the harmonic constraint imposed on the solvent waters, the motion of BHA in these two sites is more significant compared to those from complexes **1**, **4**, and **6**. It is likely that, in a solvent model without such constraints, the mobility of BHA in these two binding modes will be greater.

B. Comparison between Calculated and Experimental Properties of the BHA/HRP-C/CN Complex. Analysis of the Most Favorable Binding Mode (Complex 1). (1) Residues Lining the Binding Pocket. In its most favorable binding mode, BHA is surrounded by His42, Arg38, Pro139, Leu138, Ala140, Phe68, Pro141, Gly69, Phe179, Phe41, Phe142, Asn70, Ser73, heme methyl C18, and heme propionate C17. BHA binds in this site with its phenyl headgroup surrounded by

Table 2. *B* Factors (in Å^2) of BHA[a] and Interaction Energies[b] (in kcal/mol) of BHA with Amino Acids, Crystal Waters, and Solvent Waters in HRP-C/CN

complex **1**		complex **4**		complex **5**		complex **6**		complex **7**	
His42	−10.1	Asp182	−12.3	Arg118	−9.6	heme	−7.6	Thr288	−5.5
Arg38	−9.0	Phe142	−4.4	Gln107	−3.9	Phe68	−4.9	Asn286	−5.3
heme	−8.2	Phe179	−3.8	Ser15	−2.8	Pro141	−3.2	Ile287	−5.1
Pro139	−4.8	Pro141	−2.9	Gln106	−2.3	Ala140	−2.9	Val115	−1.0
Leu138	−3.7	Arg178	−2.6	Trp117	−1.8	Gly69	−2.8	Gly156	−1.0
Ala140	−2.6	Gln245	−1.8	Ser116	−1.7	Phe179	−1.9	Leu157	−0.8
Phe68	−1.7	Ile180	−0.9	Ile103	−0.1	Pro139	−1.8	Met284	−0.2
Pro141	−1.6	Met181	−0.5	Val119	0.0	Arg178	−0.7	Gly285	0.0
Gly69	−1.7	Phe187	−0.3	Pro4	0.1	Ser73	−0.6	Pro289	0.0
Phe179	−1.0	Ile244	0.0			Phe142	−0.4	Arg283	2.0
Ser73	−0.3	Arg183	1.1			Ala67	−0.4		
Phe41	−0.1	heme	1.7			Leu138	−0.3		
Phe142	−0.1					Asn70	−0.3		
Asn70	0.6					Ala71	−0.2		
						His42	1.1		
						Arg38	1.6		
others	−4.6	others	−4.6	others	−1.5	others	0.0	others	−4.7
protein	−48.9	protein	−31.2	protein	−23.5	protein	−25.2	protein	−21.6
X-ray H_2O	−0.1	X-ray H_2O	−0.4	X-ray H_2O	−1.6	X-ray H_2O	−3.4	X-ray H_2O	−1.2
solvent	−2.5	solvent	−15.9	solvent	−21.3	solvent	−14.5	solvent	−23.3
total	−51.5	total	−47.5	total	−46.4	total	−43.1	total	−46.1
B factor	9.6	*B* factor	20.9	*B* factor	71.5	*B* factor	21.5	*B* factor	39.8

[a] *B* factor of BHA obtained from averaging the atomic *B* factors during the last 100 ps of molecular dynamic simulations. [b] The interaction energy of each complex was calculated from the last 100 ps of the MD simulation at 2-ps intervals. Average values are reported.

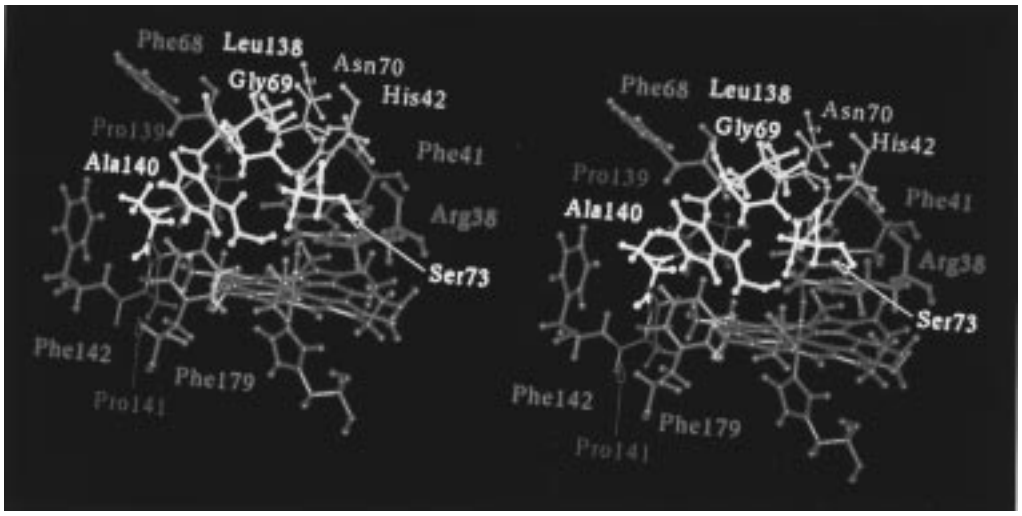

Figure 5. Stereoview of the most favorable BHA binding mode and the surrounding residues from complex **1**. In this view, the two propionate groups of the heme are toward the viewer. BHA is shown in yellow. The surrounding residues are colored differently, as indicated in this figure. The CN^- ligand is colored by atom, C in green and N in blue.

Phe68, Ala140, Pro141, and Phe179, while the hydroxamate tail is oriented toward His42 and Arg38. A number of these residues, including heme methyl C18, heme propionate C17, His42, Arg38, and Phe41 have been shown to exhibit significant perturbation in their chemical shift upon binding of BHA to HRP-C/CN.[19,26,28,30] It should be emphasized, however, that such spectral changes alone do not necessarily indicate direct residue contact and may arise as an indirect result of BHA binding. In an earlier ^{1}H NMR study of HRP-C, two upfield-shifted resonances, assigned recently to Leu138 Cβ1H and Leu138 Cδ1H$_3$,[32] exhibited significant chemical shift perturbation on complex formation with indole-3-propionic acid.[18] In addition, a recent investigation based on site-directed mutagenesis and ^{1}H NMR has definitively identified Phe179 as a key residue for the binding of aromatic donor molecules.[25] Substitution of Phe179 by Ala resulted in an 80-fold decrease in binding affinity of the cyanide-ligated enzyme for BHA compared to cyanide-ligated wild-type HRPC.[25] Phe68 and Phe142 have also been shown to modulate the binding and dynamics of the interaction between BHA and HRP-C/CN, although their roles are much less significant than that of Phe179, with binding affinity for BHA decreased only 2−3-fold when either Phe68 or Phe142 was substituted by Ala.[22,23,25] In addition, the binding mode of BHA predicted in the present study also agrees with site-directed mutagenesis data, indicating that Phe143 does not play a role in the binding of aromatic donor molecules.[22]

(2) Distances between BHA Protons and Atoms in HRP-C. ^{1}H NMR relaxation studies, 1D NOE, and 2D NOESY experiments have also been used previously to establish distance constraints between BHA protons and atoms of HRP-C.[17,21,25,26,28] To determine if the most favorable binding mode predicted from purely computational procedures was consistent with these experimental results, pairwise distances were calculated using the average value from snapshots of the last 100 ps of MD simulations for complex **1**. The results are shown in Table 3,

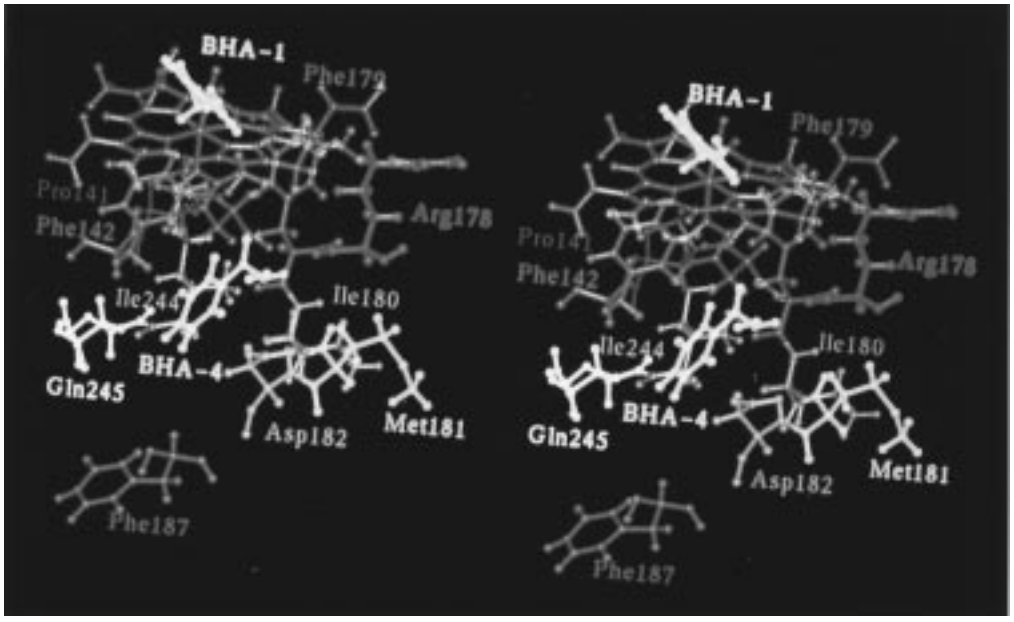

Figure 6. Stereoview of the second most favorable BHA binding mode (labeled as BHA-4) and the surrounding residues from complex **4**. The BHA binding mode from complex **1** (labeled as BHA-1) is also shown for comparison. In this view, the heme δ-meso C20 atom is toward the viewer, while the two propionate groups are pointing to the right of the figure.

Table 3. MD Average Distances[a−c] between Atoms in BHA and Atoms in HRP-C/CN in the Most Favorable (Complex **1**) and the Third Most Favorable (Complex **6**) Binding Modes

BHA/HRP-C	complex **1**	complex **6**
CδH−Fe	7.3; *8.6* (9.7)	8.2; *8.6* (9.7)
CϵH−Fe	9.6; *10.7* (10.9)	5.9; 6.4 (10.9)
CζH−Fe	*11.1* (12.0)	4.6 (12.0)
CδH−C18 methyl H	*4.0*; 7.7; *3.8*; 7.6; *3.8*; 7.5 (4.5 ± 0.5)	*4.4*; 7.1; *4.4*; 7.1; *4.5*; 7.1 (4.5 ± 0.5)
CϵH−C18 methyl H	5.5; 8.6; 5.3; 8.4; 5.3; 8.3 (3.5 ± 0.5)	*3.4*; 6.5; *3.5*; 6.5; *3.5*; 6.5 (3.5 ± 0.5)
CδH−C17^{1a}H	6.0; 9.9; 6.6; 10.1 (5.0 ± 0.5)	6.0; 9.3; 7.2; 10.2 (5.0 ± 0.5)
CϵH−C17^{1a}H	7.7; 10.9; 8.5; 11.4	4.7; 8.5; 5.5; 9.0
CδH−His42 Cϵ1H	*4.9*; 5.4 (4.5 ± 0.5)	6.3; 5.9 (4.5 ± 0.5)
CϵH−His42 Cϵ1H	6.9; 7.3 (4.5 ± 0.5)	*4.6*; 5.0 (4.5 ± 0.5)
CδH−Phe179 CδH	5.1; 8.6; 5.8; 10.0	4.7; 7.8; 5.8; 9.6
CϵH−Phe179 CδH	4.1; 8.0; 6.3; 10.3	6.0; 8.6; 5.6; 9.5
CδH−Phe179 CϵH	4.2; 7.4; 5.0; 9.0	*3.2*; 6.7; 4.6; 8.7 (2.5 ± 0.5)
CϵH−Phe179 CϵH	*2.7*; 6.6; 5.4; 9.2 (2.5 ± 0.5)	5.1; 7.8; 4.6; 8.7
CδH−Phe68 CδH	8.5; 8.3; 8.2; 6.2	7.9; 7.7; 8.1; 6.0
CϵH−Phe68 CδH	6.8; 6.6; 6.7; *4.1*	9.9; 9.8; 9.8; 8.2
CδH−Phe68 CϵH	10.7; 10.1; 10.4; 8.5	10.0; 9.6; 10.3; 8.3
CϵH−Phe68 CϵH	8.8; 8.2; 8.8; 6.4	12.1; 11.8; 12.1; 10.6
CδH−Phe142 CδH	8.3; 9.2; 9.1; 10.9	10.7; 9.8; 7.3; 7.9
CϵH−Phe142 CδH	7.0; 8.0; 8.1; 10.1	11.9; 11.1; 8.6; 9.2
CδH−Phe142 CϵH	8.0; 9.2; 8.8; 10.8	10.4; 9.1; 6.9; 7.1
CϵH−Phe142 CϵH	6.5; 7.9; 7.5; 9.8	11.9; 10.8; 8.7; 8.9
CδH−Phe41 CδH	12.0; 10.0; 9.0; 8.3	
CϵH−Phe41 CδH	14.0; 12.3; 11.2; 10.7	
CδH−Phe41 CϵH	10.8; 8.6; 7.4; 6.6	
CϵH−Phe41 CϵH	12.6; 10.8; 9.6; 9.0	

[a] Calculated from the last 100 ps of the MD simulation at 2-ps intervals. [b] For each pairwise atom−atom distance, multiple values are listed due to the fact that there are two Cδ hydrogens and two Cϵ hydrogens in each aromatic ring and three methyl hydrogens in a methyl group. [c] Experimental values, if available, are in parentheses. Those values obtained from this work that are close to the experimental values are in italic type.

with the experimental values, if available, listed in parentheses. For each pairwise atom−atom distance, multiple values are listed, due to the fact that there are two Cδ hydrogens and two Cϵ hydrogens in each aromatic ring and three methyl hydrogens in a methyl group.

For distances from the heme iron to BHA protons, obtained in the resting state of the enzyme, the MD average values agree quite well with those suggested by a ^{1}H NMR relaxation study[17] (9.7−12.0 Å). In 1D transferred NOE studies, connectivities have been documented between heme methyl C18H$_3$,[26] heme propionate C17^{1a}H,[28] and His42 Cϵ1H[28] and BHA protons. In an analysis of 2D NOESY spectra of the BHA/HRP-C/CN complex,[21] the CδH$_2$ protons of BHA showed weak connectivities with C18H$_3$ of the heme unit and with His42 Cϵ1H, indicating distance constraints of 4.5 ± 0.5 Å for these atom pairs. The corresponding MD average distances are in good agreement with these experimental data. In addition, the CϵH$_2$ protons of BHA showed medium-intensity NOE connectivities with C18H$_3$ of the heme unit (3.5 ± 0.5 Å) and a weak connectivity with His42 Cϵ1H (4.5 ± 0.5 Å). The MD average distances for these atom pairs agree less well with these constraints. For the interaction established between BHA protons and C17^{1a}H, the shortest MD average distance of 6.0 Å is slightly longer than the 5.0 ± 0.5 Å cutoff anticipated from the 1D transfer NOE experiment.[28]

2D NMR spectral analysis of the ternary complex also indicated a strong NOE connectivity between the CϵH$_2$ protons of BHA and aromatic protons of a nearby phenylalanine residue (formerly labeled as PheA),[21] indicating a distance constraint of 2.5 ± 0.5 Å. Examination of all pairwise distances between the aromatic protons of BHA and those of the four Phe residues (i.e., Phe41, Phe68, Phe142, and Phe179) in the calculated binding site uncovered a close interproton distance of 2.7 Å between one of the CϵH protons of BHA and one of the CϵH protons of Phe179. This correlates well with the strong intensity NOE observed in the 2D experiments. Full experimental validation of a Phe179 to BHA NOE connectivity requires ideally the complete assignment of all Phe179 aromatic ring protons and their respective NOE connectivities to the heme group and other residues. Nevertheless, the present results are in excellent agreement with the recent site-directed mutagenesis study, showing that Phe179 is the most significant of the

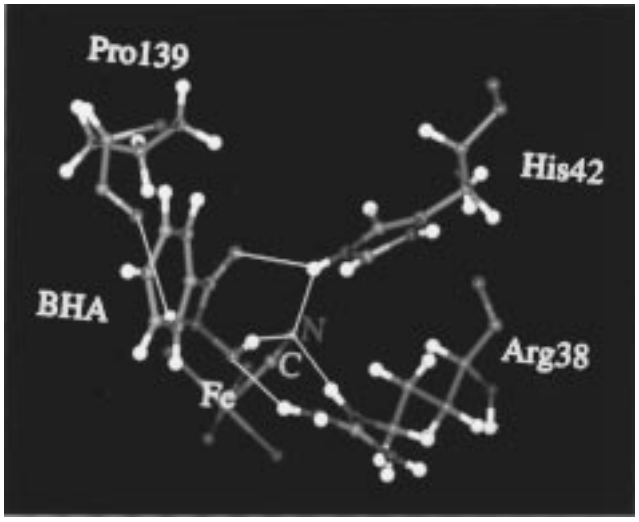

Figure 7. Polar interactions between hydroxamate polar atoms of BHA and Arg38, His42, Pro139, and the CN^- ligand in complex **1**. For clarity, only the Fe−CN fragment of the heme is shown.

aromatic residues contributing to the binding site for aromatic donor molecules.[25]

It has also been shown from 2D-NMR experiments that some substrates (such as indole-3-propionic acid and 4-methyl-BHA) interact with the side chains of two additional phenylalanine residues.[18,19,21] The results in Table 3 indicate that a number of interproton distances between BHA and the Phe68 side chain are within the 5-Å cutoff. Thus, if the binding mode predicted here is correct, one of these residues is clearly Phe68.

(3) Origin of the High Binding Affinity of BHA. To elucidate the origin of the high binding affinity of BHA to HRP-C/CN, an analysis of the H-bonding network between BHA and its surrounding residues was performed. The existence of a H-bonding network was suggested originally by Schonbaum[46] as making an important contribution to the affinity of BHA for resting-state HRP-C. In the cyanide-ligated state of HRP-C, a H-bonding network is also found to be important. Figure 7 shows that the hydroxyl group of BHA is involved in two H bonds, one as a donor and the other as an acceptor. Specifically, the hydroxyl oxygen atom of BHA forms a H bond with one of the polar hydrogens in Arg38, with an MD average distance of 1.9 Å. The hydroxyl hydrogen atom of BHA forms a H bond with the nitrogen atom of the CN^- ligand of the heme, with an MD average distance of 1.8 Å. Two other polar interactions are also identified, one of which is between the carbonyl oxygen of BHA and His42 Nϵ2H, with an average distance of 2.8 Å. The second interaction is between NH of BHA and the carbonyl oxygen of Pro139, with an MD average distance of 2.9 Å. These interactions are also reflected in the analysis of the interaction energy between BHA and these residues. The data in Table 2 confirm that the four residues that have the strongest interaction with BHA are His42, Arg38, the heme-bound CN^- ligand, and Pro139. Electrostatic interactions are found to be the dominant term in the interaction of BHA with each of these four residues, consistent with the observed H bond/polar interaction pattern. In fact, 60% of the interaction energy between BHA and HRP-C/CN is electrostatic in nature, while the remaining 40% is due to hydrophobic interaction.

(4) Comparison with X-ray Structure of BHA/ARP. Very recently, Itakura et al.[15] have reported the first X-ray structure of a complex formed between the resting state of a fungal peroxidase (ARP) and an aromatic donor molecule (BHA). The results are similar to those presented here for the ternary complex of cyanide-ligated HRP-C and BHA, as the donor molecule is located in the distal pocket of ARP with its aromatic ring positioned at the entrance of the binding channel, while the polar end is situated in the interior of the binding pocket. Furthermore, the H-bonding pattern observed experimentally in BHA/ARP is also similar, but not identical, to that established by the computational approach presented here for BHA/HRP-C/CN. In resting-state ARP, BHA forms H bonds with Arg52, His56, and Pro154 (the homologous residues to Arg38, His42, and Pro139 of HRP-C, respectively). However, small differences are seen between the two BHA complexes. In the BHA/ARP complex, the carbonyl oxygen of BHA interacts with distal Arg, rather than with distal His as in the BHA/HRP-C/CN complex. Similarly, the hydrogen bond to the oxygen atom of the hydroxyl group of BHA is provided by distal His in the BHA/ARP complex and distal Arg in the BHA/HRP-C/CN complex. In effect, the hydrogen-bonding network associated with the two key distal Arg and His side chains is reversed between these two systems. One reason for such a difference could be the presence of the cyanide ligand in BHA/HRP-C/CN that modulates the interaction between BHA and HRP-C. An additional structural feature of interest is the relative orientation of BHA in the two complexes. The X-ray structure of BHA/ARP indicates that the aromatic ring of BHA is nearly parallel to the heme, with its center of mass above the heme methyl C18 group. The binding mode of BHA to HRP-C/CN presented here indicates that the aromatic ring of BHA is at an angle ~30 Å from the heme plane and that its center of mass is in a position above the middle of the heme methyl C2 and C18 groups.

Analysis of the Second Most Favorable BHA Binding Mode (Complex 4). MD average pairwise distances between BHA atoms and HRP-C/CN atoms were calculated for BHA in the second most favorable binding mode obtained from complex **4** for comparison with those from the most favorable binding mode and with experimental results. The calculated distances between BHA aromatic protons and the heme iron, 12.1−15.9 Å, are a few angstroms longer than the results obtained by NMR relaxation methods. The distances between BHA aromatic protons and $C18H_3$, $C17^{1a}H$, His42, and Phe68 are all very large, ranging from 6.8 to 11.2 Å for $C18H_3$, 8.6 to 14.8 Å for $C17^{1a}H$, 13.3 to 17.4 Å for His42 Cϵ1H, and 12.6 to 16.8 Å for Phe68 aromatic protons. On the other hand, a few aromatic protons of three phenylalanine residues, including Phe179, Phe142, and Phe187, are within 4 Å of aromatic protons of BHA. However, none of them fall close to the 2.5 ± 0.5-Å range anticipated from NOE data for the interproton constraint between BHA and the heme-adjacent phenylalanine residue.[21] This binding mode for complex **4** does not, therefore, possess the characteristics of BHA binding indicated by experimental data and should be excluded as a realistic mode for BHA. However, the binding site identified could still be possible as a temporary radical holding site for other aromatic residues that undergo first electron oxidation. Its importance should not, therefore, be underestimated, although there is, as yet, no experimental evidence for the binding of substrate in this site. Its involvement as a temporary storage site, allowing subsequent dimerization, remains to be proven.

Analysis of the Third Most Favorable BHA Binding Mode (Complex 6). MD average pairwise distances between BHA atoms and HRP-C/CN atoms in this third most favorable binding

(46) Schonbaum, G. R. *J. Biol. Chem.* **1973**, *248*, 502−511.

mode were also calculated for comparison with those from the most favorable binding mode and with experimental results. As shown in Table 3, there is no consensus agreement with experimental results. While the binding mode in complex **6** possesses some of the characteristics of BHA binding seen from the experiments, namely the distances between BHA protons and $C18H_3$, $C17^{1a}H$, His42 $C\epsilon1H$, and the aromatic protons of the heme adjacent Phe residue (Phe179), two factors argue against this binding mode of BHA: (1) The aromatic protons of BHA in this binding mode are too close to the heme iron in comparison with experiment. (2) The polar end of BHA is pointing toward the bound and solvent water molecules, resulting in a much weaker interaction with the amino acid residues of HRP-C/CN. This mode of binding then implies a much smaller binding affinity compared with that of the binding mode represented by complex **1**.

Taken together, the results of the systematic comparison of the three most favorable sites with experiment reinforce the selection of complex **1** as the preferred binding mode of BHA. This mode was used to elucidate unresolved aspects relating to the NMR spectra of the complex.

C. Probing the Nature of the Two Interconverting Ternary Complexes Suggested by NMR. ^1H NMR studies of BHA binding to HRP-C/CN[28] have uncovered the existence of two components (designated as Y and Z) of the C18 methyl resonance at saturation. One possible explanation proposed for this observation was the existence of two forms of the BHA/HRP-C/CN ternary complex. On the basis of ^1H NMR studies of the dynamics and thermodynamics of BHA and CN^- binding, La Mar et al.[28] suggested that BHA binds in these two ternary complexes with similar binding affinity and that the two complexes interconvert at $\sim 2 \times 10^2$ s^{-1} (25 °C). Similarly, for the 2-methyl BHA derivative, two components for the $C18H_3$ resonance were resolved[21] with almost identical chemical shift values. For 3-methyl and 4-methyl BHA, it was not[21] possible to distinguish the presence of two $C18H_3$ components. Veitch and Williams[21] concluded that the two ligand-binding modes for 2-methyl BHA had exchange rates in the intermediate to slow regime, while the exchange rates for 3-methyl and 4-methyl BHAs fell in the intermediate regime.

In contrast to the behavior of the wild-type enzyme, NMR studies[22] of BHA binding to the cyanide-ligated state of the mutant F142A HRP-C showed that the ratio of the two heme methyl $C18H_3$ components at 15 °C (represented here as Y:Z) decreased from 1.4 ± 0.1 (WT) to 11.5 ± 0.5 (F142A). This indicated that, when Phe142 is mutated to Ala, BHA preferentially adopts only one of two possible binding modes found for the wild-type enzyme. Results obtained from a recent NMR study of BHA binding to F68A or F179 mutants HRP-C also provided no evidence for the existence of two binding modes.[25] This was also found to be true in the case of a parallel study involving the acidic isoenzyme of HRP, HRP A2.[24]

Results obtained from the MD simulations in this work indicate that the only two ternary complexes with the BHA aromatic protons within 5 Å of the $C18H_3$ methyl are complexes **1** and **6**. In these two complexes, BHA binds in the same position but with opposite orientations. However, the interaction energy of BHA in complex **6** is much weaker than that in complex 1, which is inconsistent with the similar binding affinity of the two BHA binding modes suggested by experiments. The binding mode in complex **6** can, therefore, be excluded as a candidate for the alternative binding mode seen from experimental data. In addition, the 1D transferred NOEs for both the Y and Z components of the heme methyl $C18H_3$ resonance to BHA were found to be similar,[28] suggesting a similar BHA orientation for the two binding modes. The consensus view is, therefore, that the two binding modes (Y and Z) seen from experimental work are not due to the orientation of BHA but rather to the orientations of the side chains of binding site residues.[22,28]

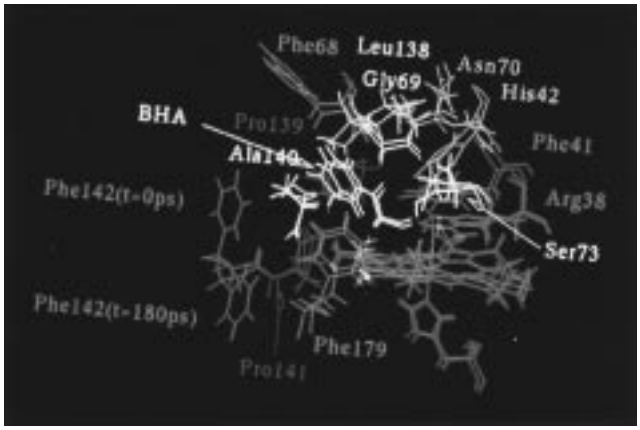

Figure 8. Movement of Phe142. Comparison of the side-chain conformation of Phe142 at $t = 0$ and 180 ps of the MD simulations. Note that other residues near the binding site show little movement during MD simulations.

The time scale of the interconversion between the two ternary complexes Y and Z at 25 °C is, at $\sim 5 \times 10^{-3}$ s,[28] much longer than the picosecond to nanosecond range used in the molecular dynamics simulations. It is not possible, therefore, to examine the conformational differences of the residues involved in the two ternary complexes. However, in the 180-ps MD simulation of complex **1**, it was found that the side chain of Phe142 underwent substantial movement, as illustrated in Figure 8. This behavior indicates a significant role for Phe142 with respect to the dynamics of BHA binding, in agreement with the mutagenesis study of the HRP-C mutant F142A.[22] On the other hand, little conformational flexibility was noted for either Phe68 or Phe179 during the 180-ps simulation. These contrasting results are consistent with the fact that Phe68 and Phe179 appear to be in close contact with the substrate in the binding site, whereas Phe142 is located at the entrance of the substrate binding channel. It is thus anticipated that a conformational change, if any, would occur over a much longer time scale for either Phe68 or Phe179.

D. Examination of Unassigned Residues in 2D NOESY Experiments. Several tentative residue assignments in earlier work have been clarified by more recent NMR studies of both resting and cyanide-ligated states of HRP-C. These include the assignment of PheW to Phe179,[25,32] PheX to Phe221,[32] IleX to Ile244,[20,29] and residue T to Leu148.[29] Results from our calculations of the residue−residue pairwise distances during MD simulation agree with the assignment of IleX and residue T. Our calculations also show that the phenylalanine side chain that was found to interact with substrate and the heme C18 methyl and originally labeled as PheA by Veitch et al.[18] and as PheW by La Mar et al.[29] is Phe179. However, it should be noted that, in a recent site-directed mutagenesis study of Phe179 mutants, it was found that one of the Phe179 resonances, is in fact, coincident with the resonances of an additional phenylalanine residue labeled as PheA.[25] Therefore, PheA is not Phe179, and its origin is unknown from the current work. The other phenylalanine residue that also interacts with substrates and which was labeled as PheB is most likely to be Phe68, according to its location relative to both the substrate and Phe179.

Conclusions

The plausible binding sites and mode of binding of BHA in cyanide-ligated horseradish peroxidase isoenzyme C have been investigated using the X-ray structure of resting-state substrate-free enzyme and purely computational methods. Specifically, using AUTODOCK, 10 initial plausible binding positions of BHA were optimized to find the best binding mode in each local region. Those five binding modes generated from AUTODOCK with the best interaction energy were selected for five separate 180-ps molecular dynamics simulations. Using the MD-averaged interaction energy between HRP-C/CN and BHA and the mobility of BHA in each plausible binding site during MD simulations as criteria, two binding sites and modes were found to be significant.

The first binding site is located in the region of the distal heme binding pocket. BHA binds in this site with its aromatic ring facing outward while its polar tail faces inward. The polar tail of BHA forms strong H bonds with Arg38 and the CN^- ligand, and it has strong electrostatic interactions with both His42 and Pro139, explaining in part the relatively high binding affinity of BHA for HRP-C/CN. The pairwise distances between atoms in BHA and atoms in HRP-C residues were measured from the MD simulations, and the majority agree well with distance constraints obtained from NMR experiments.

The second binding site is located on the proximal side of the heme plane and is only about 10 Å away from the first binding site. The pairwise distances obtained from this binding site do not agree with values obtained from NMR, indicating that BHA should not bind in this site. However, the significance of this binding site is its close proximity to the first binding site, making it a candidate site for storage of the radical product formed after the first electron-transfer step in the catalytic cycle, thereby allowing dimerization to occur after the second substrate molecule is oxidized. Although BHA is not known to form dimers following oxidation by HRP-C and, therefore, is not likely to occupy this second binding site, other aromatic donor molecules, such as phenols, which do form dimers, may occupy this predicted radical holding site. Its involvement as a temporary storage site allowing subsequent dimerization remains to be investigated experimentally.

In view of the fact that the overwhelming majority of peroxidase structures have been determined in the substrate-free form, the methods presented and validated here for the prediction of substrate binding sites and modes of BHA in HRP-C should find wide application both for other substrates that bind to the enzyme and among the members of the plant peroxidase superfamily of enzymes.

Acknowledgment. Drs. Andrew Smith, Tom Poulos, and Michael Gajhede are gratefully acknowledged for making the X-ray structure of HRP-C available for this study. The MD simulations were performed with a T-3D machine at Pittsburgh Supercomputing Center under NSF grant MCA93S007P. This research was supported by a grant from the National Science Foundation (DMB9305619) and a NATO Collaborative Research Grant CRG 931521.

JA973907E